On decomposing mixed-mode oscillations and their return maps

Christian Kuehn*

June 24, 2011

Abstract

Alternating patterns of small and large amplitude oscillations occur in a wide variety of physical, chemical, biological and engineering systems. These mixed-mode oscillations (MMOs) are often found in systems with multiple time scales. Previous differential equation modeling and analysis of MMOs has mainly focused on local mechanisms to explain the small oscillations. Numerical continuation studies reported different MMO patterns based on parameter variation. This paper aims at improving the link between local analysis and numerical simulation. Our starting point is a numerical study of a singular return map for the Koper model which is a prototypical example for MMOs that also relates to local normal form theory. We demonstrate that many MMO patterns can be understood geometrically by approximating the singular maps with affine and quadratic maps. Motivated by our numerical analysis we use abstract affine and quadratic return map models in combination with two local normal forms that generate small oscillations. Using this decomposition approach we can reproduce many classical MMO patterns and effectively decouple bifurcation parameters for local and global parts of the flow. The overall strategy we employ provides an alternative technique for understanding MMOs.

Keywords: Fast-slow system, Koper model, return map, mixed-mode oscillations, local-global decomposition.

Complex oscillatory patterns have been observed in a wide variety of applications. Analyzing these patterns from a dynamical perspective has been an active area of research for decades. However, several mathematical breakthroughs in the last 15 years have provided substantial additional insight into phenomena that describe local oscillations. In the present paper, we provide a numerical study of the singular Poincaré map in the Koper model. We demonstrate that many MMO patterns for the Koper model can already be understood just using approximations of singular limit maps. The results for the Koper model suggest that a local-global numerical simulation approach combining normal forms with discrete maps can be effective. We show that this abstract approach reproduces many typical MMO patterns that have been observed in applications. This methodology aims to close a gap between previous numerical studies of MMO patterns and analytical results about local normal forms.

1 Introduction

Mixed-mode oscillations (MMOs) are patterns of small and large amplitude oscillations in a time series that differ at least by one order in magnitude. They have been observed experimentally in

*Max Planck Institute for the Physics of Complex Systems

the Belousov-Zhabotinsky reaction in the 1970's and 1980's [39, 54] and have been encountered more recently in a wide variety of different experiments [37, 38, 61, 19]. The basic classification has been based on counting the number of small oscillations s and large oscillations L so that we can symbolically represent an MMO by

$$\dots L_{j-1}^{s_{j-1}} L_j^{s_j} L_{j+1}^{s_{j+1}} \dots$$

where $j \in \mathbb{N}$ is an index. For example, if we have a periodic time series that has 2 large amplitude oscillations (LAOs) and then 3 small amplitude oscillations (SAOs) we get $\dots 2^3 2^3 2^3 \dots$ or simply an MMO of type 2^3. Systems exhibiting MMOs are often modeled using differential equations [12, 3]. Local bifurcation theory [10, 29] and numerical methods [45, 18] have been developed to gain a lot of insights into SAO generating mechanisms [9]. A multiple time scale structure of the system is a key component for many local mechanisms. A detailed survey of this theory and its applications to particular models has been completed recently [15]. The main findings of many numerical studies (see e.g. [45, 73, 62, 17]) and experiments (see e.g. [39, 53, 70]) are transition sequences of periodic orbits; for example, if we only consider MMOs with patterns of the form $\cdots L^s L^s \cdots$ such a transition sequence can be represented as follows

$$\cdots \to (L_{p_1})^{s_{p_1}} \to (L_{p_2})^{s_{p_2}} \to (L_{p_3})^{s_{p_3}} \to \cdots \tag{1}$$

where p is a control/bifurcation parameter i.e. under variation of a single parameter changing patterns of MMOs can be observed. To understand patterns of the form (1) several approaches have been used. The theory of local normal forms has been applied to explain the SAOs and then it is usually assumed that the global return mechanism satisfies certain properties (see e.g. [73, 10]) so that the local theory becomes applicable or a phenomenological model for the return map is proposed [58, 59]. Another approach is to compute Poincaré maps [52] numerically under parameter variation (see e.g. [42, 56, 33]) to explain transitions of MMO patterns or to use numerical continuation [46] to subdivide parameter space (see e.g. [45, 18]). These techniques have provided tremendous insight into what types of sequences (1) can be found in different systems. However, all previously mentioned studies vary parameters in such a way that local and global dynamics change *simultaneously*. Here we suggest that to understand which patterns of the form (1) occur one also has to ask what happens when this parameter coupling is not present. Only in this context one is able to distinguish the effects of parameter variation on the local normal form from the variation of parameters in the Poincaré map. We start by applying this idea in the context of Koper's model [45]. For Koper's model the local dynamics is well-understood [15] and SAOs are generated by folded nodes [67, 71] and folded saddle-nodes of type II (or singular Hopf bifurcation, [29, 15]) which are normal forms for systems fast-slow systems with three variables (see also Appendices A.2-A.3 for a brief review).

Remark: We point out that folded nodes and singular Hopf bifurcation are two possible normal forms under the assumptions of fast-slow systems structure and non-degeneracy assumptions for a folded critical manifold. Obviously one can also suggest other possible SAO mechanisms [35, 56]. However, we have chosen to focus on the Koper model that is well-described locally by the two normal forms described above. The main reasons for this choice are that many experimental and analytical studies have been found that exhibit folded nodes and/or singular Hopf bifurcation (see the review [15] for a list systems with folded nodes and singular Hopf bifurcation). Furthermore, it has recently been shown that both mechanisms also relate to delayed Hopf bifurcation [50] which has been proposed as another SAO mechanism.

The global return mechanism for MMOs in the Koper model is provided by a cubic relaxation-oscillation mechanism [44, 68] that has already been investigated by van der Pol in the 1920s [13, 14]. Here we provide numerical computations of the global Poincaré return map as a composition of several maps in the singular limit of perfect time scale separation. These calculations reveal that the return map can be surprisingly regular. Using affine and quadratic approximations to the singular maps we investigate MMO patterns and find that the approximations suffice to understand MMO sequences observed in extensive numerical continuation. Motivated by these results we combine two local normal form ODEs with abstract linear and quadratic maps to study MMOs. It is shown that classical sequences of the form (1) as well as chaotic MMOs can be easily generated in this framework. In particular, it is easy to design MMO patterns and to understand the differences in local and global parameter effects. We point out that this study also contributes to closing the gap between numerical simulation and local normal forms by reproducing several of the MMO transition sequences observed by a simultaneous local and global parameter variation in the Koper model.

The paper is structured as follows. Appendix A contains the necessary background for readers not familiar with fast-slow system and MMO generating mechanisms in these systems. The main part of this paper starts in Section 2 where the Koper model is introduced and its basic properties are reviewed. In Section 3 the global singular return map for the Koper model is decomposed into several more tractable flow maps using numerical simulations. In Section 4 the maps are approximated by affine and quadratic map models; Appendix B contains a discussion of the approximation error. In Section 5 the global aspects of MMOs in the Koper model are analyzed using the flow map models. In Section 6 we consider a standard local-global decomposition of the MMO generating mechanisms. The key point is that we suggest to separate the parameter dependencies for the local and global models. We combine a global return map model with local SAOs induced by folded node and singular Hopf normal forms. We conclude with a brief outlook, describing the wider applicability of our approach, in Section 7.

2 The Koper Model

One version of the Koper model for MMOs is given by

$$\begin{aligned} \epsilon_1 \dot{x} &= y - x^3 + 3x, \\ \dot{y} &= kx - 2(y+\lambda) + z, \\ \dot{z} &= \epsilon_2(\lambda + y - z), \end{aligned} \tag{2}$$

where (k, λ) are the main bifurcation parameters and (ϵ_1, ϵ_2) are the singular perturbation parameters. The equations were first studied as a two-dimensional model by Boissonade and De Kepper [7] modeling a prototypical chemical reaction. Koper [45] added a third variable to a planar system and used numerical continuation techniques [26, 21] to study MMOs [45]. It is very important to note that equations similar or equivalent to (2) have been proposed many times *independently* by several different research groups [25, 66, 43, 10, 47, 29] as a "canonical", "minimal" or "typical" model for MMOs. The version (2) of Koper's model was proposed by the author and co-workers in [15]; it is obtained by a coordinate transformation of Koper's original model and has the symmetry

$$(x, y, z, \lambda, k) \mapsto (-x, -y - z, -\lambda, k)$$

which allows us to restrict to parameter regions with $\lambda \geq 0$ or $\lambda \leq 0$ without loss of generality. Here we shall only review the local bifurcation structure briefly an introduce the necessary notation; a

detailed local fast-slow systems analysis of (2) can be found in [15]. We also point out that the terminology reviewed in Appendix A will be assumed from now on.

If $0 < \epsilon_{1,2} \ll 1$ holds then (2) is a three time-scale system. We shall focus on the case $\epsilon_2 = 1$ and $0 < \epsilon_1 =: \epsilon \ll 1$ in which case we have one fast variable x and two slow variables (y, z). The critical manifold is

$$C_0 = \{(x, y, z) \in \mathbb{R}^3 : y = x^3 - 3x =: c(x)\}.$$

The typical cubic (or S-shaped) structure splits the critical manifold into several parts

$$C_0 = C^{a,-} \cup F_- \cup C^r \cup F_+ \cup C^{a,+}$$

where $C^{a,-} := C \cap \{x < -1\}$, $C^{a,+} := C \cap \{x > 1\}$ are normally hyperbolic attracting, $C^r := C \cap \{-1 < x < 1\}$ is normally hyperbolic repelling and

$$F_- := C \cap \{x = -1\} = \{(-1, 2, z)\} \qquad \text{and} \qquad F_+ := C \cap \{x = 1\} = \{(1, -2, z)\}$$

are fold curves curves of the critical manifold. MMOs can easily be observed in simulations; see Figure 1. The desingularized slow subsystem is

$$\begin{aligned} \dot{x} &= kx - 2(c(x) + \lambda) + z, \\ \dot{z} &= (3x^2 - 3)(\lambda + c(x) - z). \end{aligned} \tag{3}$$

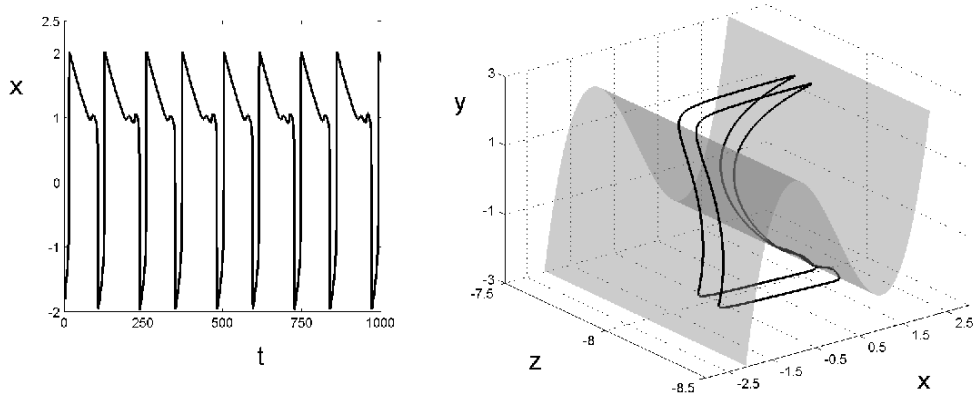

Figure 1: The parameter values for the simulation are $(\epsilon, k, \lambda) = (0.01, -10, -7)$. The time series for a $1^1 1^2$ MMO for the variable x is shown on the left and the phase space trajectory is shown on the right; the critical manifold C_0 is shown in grey.

There are two folded singularities

$$p_\pm = (\pm 1, 2\lambda \mp (4 + k)).$$

By symmetry we shall only focus on the folded singularity p_+. The linearization of the desingularized slow flow p_+ is

$$\begin{pmatrix} \dot{X} \\ \dot{Z} \end{pmatrix} = \begin{pmatrix} -10 & 1 \\ -6(8 + \lambda) & 0 \end{pmatrix} \begin{pmatrix} X \\ Z \end{pmatrix} =: A_+ \begin{pmatrix} X \\ Z \end{pmatrix} \tag{4}$$

where we already set $k = -10$ which will fixed from now on. Note that in this case $\{X = 0\}$ corresponds to the fold line F_+ and p_+ is located at the origin. The eigenvalues of A_+ are

$$\sigma_w(\lambda) = -5 + \sqrt{-23 - 6\lambda} \qquad \text{and} \qquad \sigma_s(\lambda) = -5 - \sqrt{-23 - 6\lambda},$$

with associated eigenvectors

$$\Sigma_w(\lambda) = \begin{pmatrix} \frac{1}{5+\sqrt{-23-6\lambda}} \\ 1 \end{pmatrix} \qquad \text{and} \qquad \Sigma_s(\lambda) = \begin{pmatrix} \frac{1}{5-\sqrt{-23-6\lambda}} \\ 1 \end{pmatrix}.$$

Therefore p_+ is a folded saddle for $\lambda < -8$, a folded saddle-node of type II (FSN II [67, 15]) for $\lambda_{\text{FSN II}} = -8$ and a folded node for $\lambda \in (-8, -23/6)$. At $\lambda_{nf} = -23/6$ the transition from a folded node to a folded focus occurs. The singular Hopf bifurcation for the full system occurs $O(\epsilon)$ away from $\lambda_{\text{FSN II}}$. It is supercritical and the stable global equilibrium q loses stability at this point. Therefore the interesting parameter region for MMOs is

$$\lambda \in (\lambda_{\text{FSN II}}, \lambda_{nf}) = (-8, -23/6), \qquad k = -10.$$

Note that this parameter region represents a typical one-parameter MMO sequence [45, 15]. The important eigenvector for global returns is Σ_s associated to the strong primary canard γ_s as it bounds the rotational sectors lying on $C^{a,+}$. The x-component Σ_s^x of Σ_s lies, for the scaling we have chosen, between $\Sigma_s^x(-8) = \infty$ and $\Sigma_s^x(-23/6) = \frac{1}{5}$. Therefore the rotational sectors [10] that subdivide the funnel region are given by a convex cone with opening angle between $\frac{\pi}{2}$ and $\cos^{-1}(25/26)$.

3 Return Maps - Decomposition

Our goal is to analyze the structure of the global singular return map. Instead of using the standard approach of computing the Poincaré map between two fixed sections [64, 31, 52] we are going to decompose the map according to fast-slow systems theory (see e.g. [36, 34, 68] for this approach). We fix $\epsilon = 0$ and recall that $k = -10$. Then we focus on λ as the primary bifurcation parameter. In this case the folded node p_+ and the unique equilibrium q account for the SAOs. Observe that global returns to a neighborhood of p_+ can be decomposed. See Figure 2 for an illustration of the one-dimensional singular maps we are going to define:

(a) Trajectories can reach the fold line F_+ at a jump point and follow the fast flow to the drop curve $L^{a,-} := C \cap \{x = -2\}$. Then trajectories follow the slow flow induced by (3) to F_- and jump to the drop curve $L^{a,+} := C \cap \{x = 2\}$. We denote this map by

$$m_j : F_+ \to L^{a,-} \to F_- \to L^{a,+}$$

where j indicates that we consider a regular jump. We denote the intermediate map by $m_{a-} : L^{a,-} \to F_-$. Observe that if we parametrize the domain and range by z then the intermediate map m_{a-} is the only non-trivial component of the map m_j and the other parts of m_j are the identity with respect to z.

(b) Trajectories can flow into the folded node p_+. Suppose we consider trajectories tracking the part of the strong canard γ_s contained in C^r. These trajectories jump at some point from γ_s to $C^{a,-}$ and flow into F_- before jumping to $L^{a,+}$. Denote this map by

$$m_f : \gamma_s \to C^{a,-} \to F_- \to L^{a,+}$$

where f indicates a jump forward (or away) singular canard orbit; again observe that only the part $C^{a,-} \to F_-$ is non-trivial with respect to z.

(c) Trajectories tracking the strong canard $\gamma_s \subset C^r$ can also jump at some point from γ_s to $C^{a,+}$ and flow into F_+. It will be advantageous to terminate this map at a line $L^\mu := C \cap \{x = 1+\mu\}$ for some $\mu \geq 0$ sufficiently small. Then we have a map

$$m_b : \gamma_s \to C^{a,+} \to L^\mu$$

where b indicates a jump backwards (or back) singular canard orbit.

(d) There is also a map induced by the slow flow on $C^{a,+}$ starting from the drop curve $L^{a,+}$ towards the fold line

$$m_{a,+} : L^{a,+} \to L^\mu$$

(e) The linearization (4) at the folded singularity p_+ can be used to define a flow map in the fold region

$$m_s : L^\mu \to F_+$$

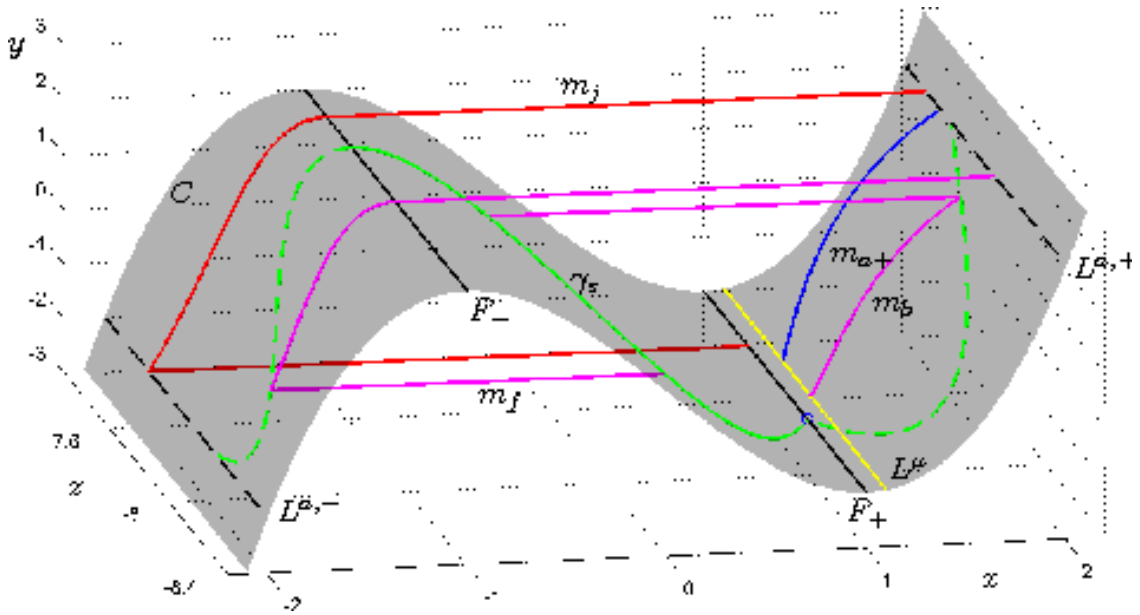

Figure 2: Illustration of the singular map decomposition; parameter values are $(\epsilon, k, \lambda) = (0, -10, -7)$. Definitions of all maps and domains are given at the beginning of Section 3. Here we show: the critical manifold C (grey), the strong canard $\gamma_s \subset C^m$ (green) and its projections to $C^{a,\pm}$ (dashed green), the fold lines $F_\pm$ (black) and their projections $L^{a,\mp}$ (dashed black, $\mu = 0.1$), the line L^μ (yellow) and the folded node p_+ (blue circle). Examples for the maps m_j (red, regular jump), $m_{a,+}$ (blue, flow towards F_+), m_f (magenta, jump forward canard) and m_b (magenta, jump backward canard) are displayed as well.

Figure 3 shows representatives of the maps m_j, $m_{a,+}$, m_b and m_f for $\lambda = -7$ with respect to the variable z and also the associated slow flows. The main observation is that the maps are surprisingly regular.

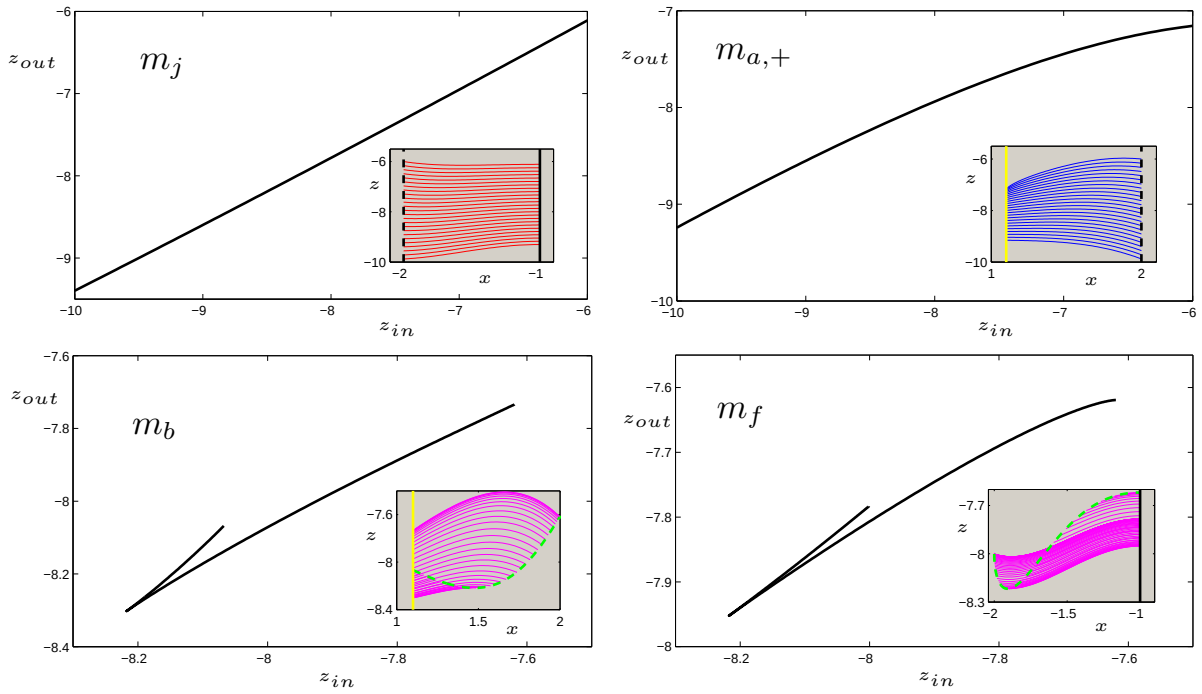

Figure 3: Singular maps for $(k, \lambda) = (-10, -7)$ with respect to the z-variable i.e. the horizontal axis shows $z = z_{in}$ and the vertical axis shows $z_{out} = m_K(z_{in})$ for $K \in \{j, (a, +), b, f\}$. The insets (grey background) illustrate the phase space flow on the attracting critical manifolds $C^{a,\pm}$ associated to the maps m_K; we show only every tenth trajectory in the computation of m_K. The color coding is the same as in Figure 2.

4 Return Maps - Modeling

In this section we are going to discuss the modeling of the maps computed in Figure 3; a discussion of the approximation error as well as the error for $\epsilon > 0$ is given in Appendix B. Figure 3 motivates considering affine and/or quadratic maps. The map m_j seems to be close to an affine map which is due to the very simple regular slow flow from $L^{a,-}$ to F_-; see also Figure 2. Similarly, we propose to model the map $m_{a,+}$ by a quadratic map. The maps induced from the projections of the strong canard $\gamma_s \subset C^r$ onto $C^{a,\pm}$ are multi-valued when parametrized with respect to z due to the fold structure of γ_s; see Figure 2. With another parametrization we expect that m_b and m_f are generically single-valued by uniqueness of solutions for the desingularized slow subsystem. The parametrization with respect to z is very convenient. We propose to make the following ansatz:

$$m_K(z) = c_2(\lambda)z^2 + c_1(\lambda)z + c_0(\lambda)$$

for each map m_K with $K \in \{j, (a, +), b, f\}$ where the coefficients $c_{0,1,2}(\lambda)$ are to be determined. We are going to illustrate the procedure for finding the coefficients for m_f and just state the results we obtained for the other three maps. The ansatz is that m_f can be decomposed as follows:

$$m_f(z) = \begin{cases} c_1^{fu}(\lambda)z + c_0^{fu}(\lambda) & \text{if } z_{min}^{fu}(\lambda) \le z \le z_{max}^{fu}(\lambda), \\ c_2^{fl}(\lambda)z^2 + c_1^{fl}(\lambda)z + c_0^{fl}(\lambda) & \text{if } z_{min}^{fl}(\lambda) \le z \le z_{max}^{fl}(\lambda), \\ \text{undefined} & \text{otherwise,} \end{cases} \tag{5}$$

where we impose continuity at the shared boundary point $m_f(z_{min}^{fu}) = m_f(z_{min}^{fl})$. See Figure 4 for an example. In Figure 4 the upper part of m_f is approximated by an affine map and the lower part

by a quadratic. The computation of the approximation error in Appendix B for $\lambda \in (\lambda_{\text{FSN II}}, \lambda_{nf})$ shows that for each fixed value of λ the affine and quadratic models provide an approximation on the order of 10^{-2} of the singular maps obtained via numerical integration of slow flow trajectories on a fine mesh.

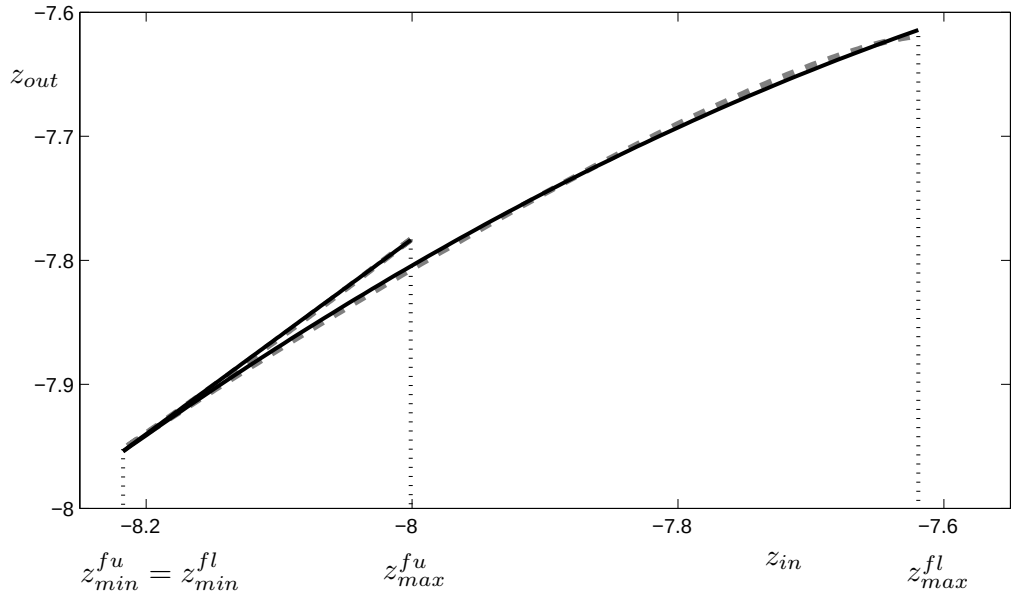

Figure 4: Singular map m_f with $z_{out} = m_f(z_{in})$. The computed map is shown as a dashed grey curve and the approximations are shown in solid black (affine for upper part and quadratic for lower part). The bounds of the domains for each part of the map are marked as well (dotted vertical lines).

As a next step we investigate all functions depending on λ in (5). The boundary z_{max}^{fu} is given by the folded singularity p_+ so that $z_{max}^{fu}(\lambda) = 2\lambda + 6$. We also know from the definition of (5) that $z_{min}^{fu} = z_{min}^{fl}$. The other functions of λ can only be approximated numerically due to the nonlinear slow flows on C^r, which defines γ_s, and on $C^{a,-}$, which defines the map to F_-. Figure 5 shows numerical computations of the unknown functions of λ in the definition of m_f in (5).

Several observations can be made from Figure 5 and the previous remarks. All the domain boundaries $z_{min}^{fu}(\lambda)$, $z_{max}^{fu}(\lambda)$, $z_{min}^{fl}(\lambda)$ and $z_{max}^{fl}(\lambda)$ are very regular and seem to depend almost linearly on λ. The coefficients of the linear and quadratic polynomials have substantial nonlinear dependencies on λ for the entire range $\lambda \in (\lambda_{\text{FSN II}}, \lambda_{nf})$. This implies that although affine and quadratic maps can be very good approximations at fixed parameter values it will be more difficult to analyze the global return maps inducing MMOs as parameter-dependent families. For the other maps m_b, m_j and $m_{a,+}$ we propose the following approximations:

$$m_b(z) = \begin{cases} c_2^{bu}(\lambda)z^2 + c_1^{bu}(\lambda)z + c_0^{bu}(\lambda) & \text{if } z_{min}^{bu}(\lambda) \le z \le z_{max}^{bu}(\lambda), \\ c_1^{bl}(\lambda)z + c_0^{bl}(\lambda) & \text{if } z_{min}^{bl}(\lambda) \le z \le z_{max}^{bl}(\lambda), \\ \text{undefined} & \text{otherwise,} \end{cases} \tag{6}$$

$$m_j(z) = c_1^j(\lambda)z + c_0^j(\lambda), \tag{7}$$

$$m_{a,+}(z) = c_2^a(\lambda)z^2 + c_1^a(\lambda)z + c_0^a(\lambda), \tag{8}$$

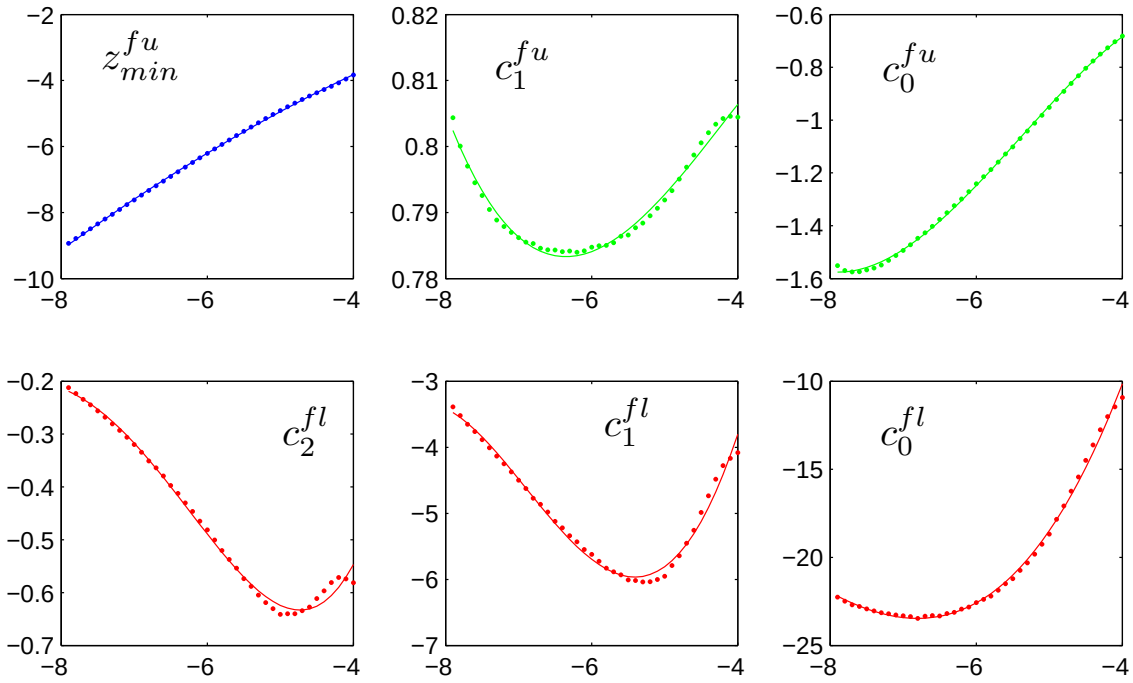

Figure 5: Horizontal axes are λ and vertical axes are the respective coefficients e.g. top left figure shows $z_{min}^{fu}(\lambda)$. The only relevant part for the definition of (5) that is not shown is z_{max}^{fl} which is as regular (almost linear) as the other parts of the domain boundaries for m_f. The dots are computed points and the curves provide polynomial fits (quadratic=blue, cubic=green and quartic=red).

where we impose continuity at the shared boundary point for m_b i.e. $m_b(z_{min}^{bu}) = m_b(z_{min}^{bl})$. As a next step we are going to calculate the map for the linearized desingularized slow flow near p_+. The intersection of the eigendirection of Σ_s with $L^\mu = \{x = 1 + \mu\}$ is easily calculated as

$$(1, 2\lambda + 6)^T + \left(\mu, \frac{\mu}{\Sigma_s^x(\lambda)}\right)^T = (1 + \mu, 2\lambda + 6 + \mu(5 - \sqrt{-23 - 6\lambda})) =: (1 + \mu, z^\mu(\lambda)).$$

Hence all trajectories that arrive at L^μ with $z \geq z^\mu(\lambda)$ will stay in the funnel and reach p_+ while trajectories for $z < z^\mu(\lambda)$ will first reach the fold line F_- and jump to $L^{a,-}$. To see where on F_+ the last class of trajectories ends up we could just solve (4). Note however that there exists an approximation for $z < z^\mu(\lambda)$ that just amounts to projecting $(\mu, Z(0))$ parallel to Σ_s onto $\{X = 0\}$ which is given by

$$(\mu, Z(0)) \mapsto \left(0, Z(0) - \frac{\mu}{\Sigma_s^x}\right).$$

Therefore we get the local representation for the map m_s in (X, Z)-coordinates

$$m_s^{loc}(Z) = \begin{cases} 2\lambda + 6 & \text{if } z \geq z^\mu(\lambda), \\ 2\lambda + 6 + Z - \frac{\mu}{\Sigma_s^x} & \text{if } z < z^\mu(\lambda). \end{cases}$$

If z is the coordinate obtained in original coordinates without linearization then

$$m_s(z) = \begin{cases} 2\lambda + 6 & \text{if } z \geq z^\mu(\lambda) \\ z - \frac{\mu}{\Sigma_s^x} & \text{if } z < z^\mu(\lambda) \end{cases}$$

where the error is $\mathcal{O}(\mu)$ as $\mu \to 0$. With the different maps available we can proceed to analyze how they can be used to explain the global returns that generate LAOs.

5 Mixed-Mode Oscillations

Throughout this section we work with the polynomial approximations to the maps $m_{(.)}$ that have been derived in the last section. The first question we shall consider is what happens to trajectories that do not follow the canard $\gamma_s \subset C^r$ when arriving at p_+ or which land outside of the funnel region. The relevant map for this purpose is

$$(m_{a,+} \circ m_j) : F_+ \cap \{z \leq 2\lambda + 6\} \to L^\mu \tag{9}$$

We are interested when part of the domain of (9) is returned inside the funnel so that $(m_{a,+} \circ m_j)(z) > z^\mu(\lambda)$. Figure 6 shows the map (9) for three different values of λ. We observe that closer to the folded saddle-node of type II (i.e. near the singular Hopf bifurcation) trajectories that arrive outside the funnel on F_+ can get mapped back into the funnel under (9). For $\lambda = -6.5$ in Figure 6 we observe that no trajectories can return into the funnel and that the return map $(m_s \circ m_{a,+} \circ m_j)$ will have a stable fixed point since μ is small and hence the projection m_s will preserve the intersection with the diagonal.

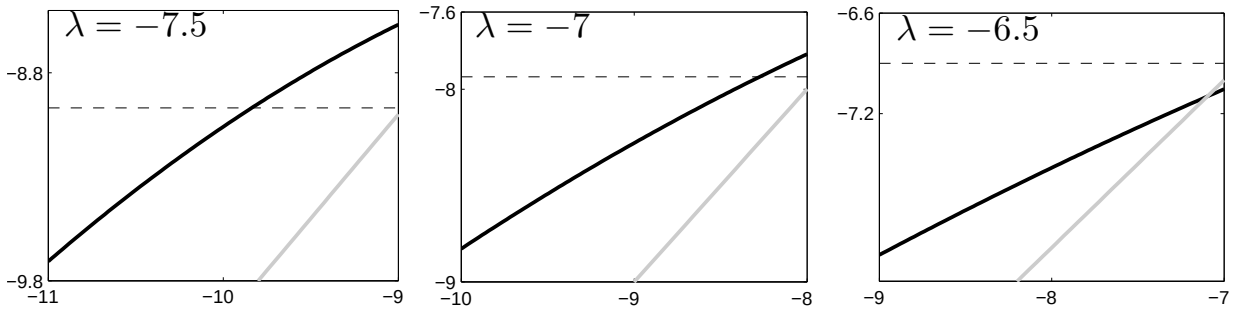

Figure 6: Map $(m_{a,+} \circ m_j)(z)$, approximated by (7) and (8) with $k = -10$ and $\mu = 0.1$. Horizontal axes are input z-coordinates on a domain $z \in ((2\lambda + 6) - 2, 2\lambda + 6) \subset F_+$ and vertical axes are $(m_{a,+} \circ m_j)(z)$ (think black curves). The location of the folded node funnel region $z^\mu(\lambda)$ is shown by horizontal dashed black lines and the diagonal is indicated by the thick grey line.

Hence we can consider several quantitative questions:

1. For what values of λ do trajectories from outside the funnel re-enter it?
2. When does the map $(m_s \circ m_{a,+} \circ m_j)$ have fixed points? When does the fixed point coincide with the folded node p_+?
3. How are trajectories mapped into the funnel? More precisely, what is the dependence of the distance δ to the strong singular canard $\gamma_s \cap C^{a,+}$ upon varying λ?

A trajectory starting for $z < 2\lambda + 6$ will re-enter the funnel after one global return if and only if

$$\begin{aligned}(m_{a,+} \circ m_j)(z) &= c_2^a(\lambda)(c_1^j(\lambda)z + c_0^j(\lambda))^2 + c_1^a(\lambda)(c_1^j(\lambda)z + c_0^j(\lambda)) + c_0^a(\lambda) \\ &= c_2^a(c_1^j)^2 z^2 + \left(2c_2^a c_1^j + c_1^a c_1^j\right) z + (c_0^j)^2 c_2^a + c_1^a c_0^j + c_0^a < z^\mu(\lambda)\end{aligned}$$

By monotonicity of (9) on the required interval (see Figure 6) we can just pick the folded node $z = 2\lambda + 6$ and determine when the condition fails; this yields the critical parameter value at which

not all trajectories near p_+ return to the funnel in one iteration. We find that the parameter value at which p_+ gets returned to the boundary of the funnel is $\lambda = \lambda_r \approx -6.7887$. Next, we consider the fixed points of $(m_s \circ m_{a,+} \circ m_j)$. Those points correspond to candidates representing relaxation oscillations. We find that at $\lambda = \lambda_r$ a stable fixed point appears for the map $(m_s \circ m_{a,+} \circ m_j)$. Therefore we find that a transition to relaxation oscillations occurs near λ_r for the full system and ϵ sufficiently small; this can be confirmed by numerical continuation [15]. Note that the bifurcation that creates the fixed point occurs at the boundary of the domain of $(m_s \circ m_{a,+} \circ m_j)$.

As a next step we consider candidates that follow the canard $\gamma_s \cap C^r$ i.e. we consider the maps m_f and m_b. We start with m_b which represents medium-size canard-induced oscillations if trajectories from the domain of m_b re-enter the funnel after one iteration step. Figure 7 plots three examples of the map m_b. The closer the parameter values are to the folded saddle-node of type II at $\lambda = -8$ the larger is the part of $\gamma_s \cap C^r$ that returns inside the funnel. The closer we are to relaxation oscillation at $\lambda = \lambda_r$ the more of $\gamma_s \cap C^r$ gets mapped outside the funnel.

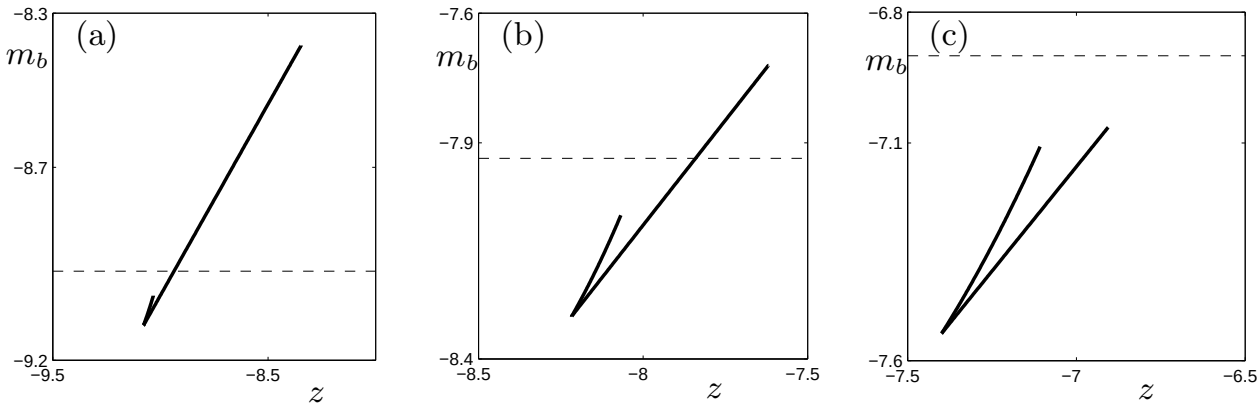

Figure 7: Singular maps with respect to the z-variable i.e. the horizontal axis shows $z = z_{in}$ and the vertical axis shows $m_b = m_b(z_{in})$. The horizontal dashed line indicates the funnel boundary $z^\mu(\lambda)$; here $\mu = 0.1$. (a) $\lambda = -7.5$, (b) $\lambda = -7$ and (c) $\lambda = -6.5$.

Note that near $\lambda = -8$ with $\lambda > -8$ we must always have some part of $\gamma_s \cap C^r$ near p_+ that does get mapped outside the funnel since the opening cone angle of the funnel region is less than $\frac{\pi}{2}$; see Section 2. Therefore there is always one part inside and one part outside the funnel for jump back canard orbits. Orbits in the full system that follow γ_s^ϵ for an $O(1)$-time on the slow time scale and get mapped back to $C^{a,+}$ via perturbation of m_b represent intermediate oscillations.

For the map m_f we immediately consider $m_{a,+} \circ m_f$ to see how jump forward canards get returned relative to the funnel. Figure 8 shows that there is a very rapid transition from jump forward canards that end all in the funnel for $\lambda = -7$ (Figure 8(a)), a splitting of jump forward canards with respect to the funnel (Figure 8(b)) and all jump forward canards outside the funnel for $\lambda = -6.6$ (see Figure 8(c)). Let us consider the case when the entire jump forward canards end up in the funnel. This can be interpreted as a global MMO generating mechanism via canards. More precisely, a trajectory of the full system can make small oscillations near a folded node, follow $C^r \cap \gamma_s$ closely producing an intermediate oscillation and then return into the funnel. This provides a mechanism to transition small loops into large ones via canards. The closer we get to $\lambda = \lambda_r$ the more excursions outside the funnel occur which means that in this region we expect more mixed

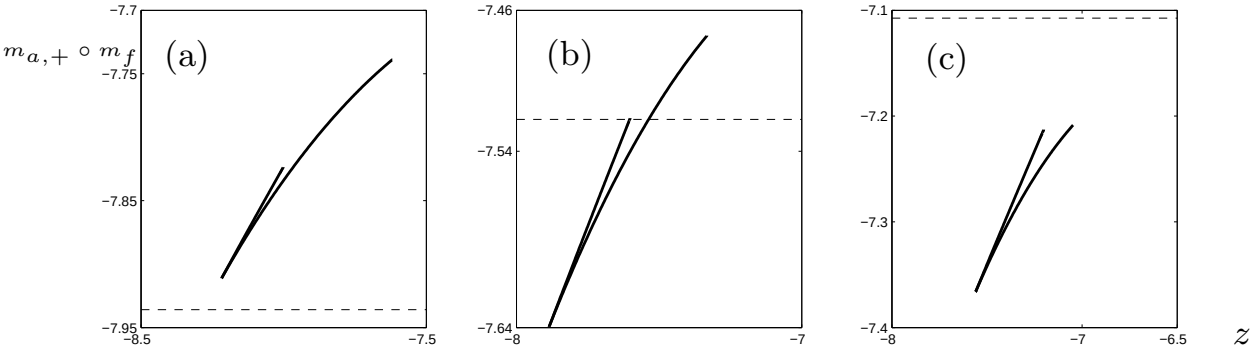

Figure 8: Singular maps with respect to the z-variable i.e. the horizontal axis shows $z = z_{in}$ and the vertical axis shows $m_{a,+} \circ m_f = (m_{a,+} \circ m_f)(z_{in})$. The horizontal dashed line indicates the funnel boundary $z^\mu(\lambda)$; here $\mu = 0.1$. (a) $\lambda = -7$, (b) $\lambda = -6.8$ and (c) $\lambda = -6.6$.

behavior of MMOs of type L^s with $L > 1$. It is also expected that period-doubling bifurcations of the return map can explain transitions between regions of different LAOs. Since resonances for the eigenvalues [71] of the folded node are fewer near λ_r we also expect s to decrease if we increase λ. Hence we find that MMO sequences near a singular Hopf bifurcation will produce patterns with $s \gg 1$ and small L while away from the singular Hopf L^s patterns with $L \sim s$ are more likely to occur. All these findings agree with numerical continuation results in [45, 15].

Therefore one main conclusion from the numerical simulations considered here is that the singular limit decomposition is already sufficient to explain many MMO transition sequences. Indeed, in the singular limit we could already identify the local normal forms (see Section 2 and [15]) and here we calculated a decomposition of the global return map. The main point is that we have used a different, and easily implementable, numerical *technique* to understand geometrically many of the MMO patterns that have been found using extensive numerical continuation runs [45].

6 A Local-Global Model

We have seen that the global singular return maps for the Koper model are very regular and can often be described as affine or quadratic maps. The only feature of the global returns that is complicated to describe are canard orbits that follow the strong canard $\gamma_s \cap C^r$. These orbits describe intermediate oscillations i.e. orbits that, under parameter variation will grow to a large relaxation loop or decay to a small oscillation. However, many MMO transitions can be understood without these orbits as shown in the previous section. Hence it is natural to ask what happens if we do not consider these intermediate orbits and look at a simulation model for MMOs containing local and global maps. The local description of this model is chosen as a flow map for a folded node or a folded-saddle node ODE normal form; see Appendix A. We assume without loss of generality that the folded singularity is located at the origin $(x, y, z) = (0, 0, 0)$. For the local dynamics we use the normal forms (15) and (18). Recall that the critical manifold of both normal forms is

$$C_0 = \{(x, y, z) \in \mathbb{R}^3 : y = x^2\}$$

It is attracting for $x > 0$ and repelling for $x < 0$ and we denote the two branches of C_0 by C_0^a and C_0^r. The associated attracting slow manifold provided by Fenichel Theory is

$$C_\epsilon^a = \{(x, y, z) \in \mathbb{R}^3 : x = h_\epsilon^a(y, z)\}$$

where the map h^a_ϵ is given by the implicit function theorem and $h^a_0(y,z) = \sqrt{y}$. Define two sections

$$\begin{aligned}\Sigma_1 &:= \{(x,y,z) \in \mathbb{R}^3 | x = k_1\} \\ \Sigma_2 &:= \{(x,y,z) \in \mathbb{R}^3 | x = -k_2\}\end{aligned}$$

for suitable fixed $k_j > 0$, $k_j = O(\sqrt{\epsilon})$ with $j = 1, 2$. The choice of scaling $O(\sqrt{\epsilon})$ is prescribed by the fact that outside of a neighborhood of size $O(\sqrt{\epsilon})$ of the origin Fenichel Theory applies. Define a map

$$m_{12} : \Sigma_1 \to \Sigma_2 \tag{10}$$

by the flow map of (15) or (18). Note that the sections Σ_j are naturally parametrized by the coordinates (y, z). The global return map $m_{21} : \Sigma_2 \to \Sigma_1$ will be modeled as follows:

$$\begin{aligned}m_{21}(y,z) &= \begin{pmatrix} k_1^2 \\ m(z) \end{pmatrix} + \epsilon \left[\begin{pmatrix} a_{11} & a_{12} \\ a_{21} & a_{22} \end{pmatrix} \begin{pmatrix} y \\ z \end{pmatrix} + \begin{pmatrix} b_1 \\ b_2 \end{pmatrix} \right] + O(\epsilon^2) \\ &= (k_1^2, m(z))^T + \epsilon[A(y,z)^T + b] + O(\epsilon^2) \end{aligned} \tag{11}$$

where $m(z) = m_2 z^2 + m_1 z + m_0$ and we require that the matrix A is invertible. Note that we can make several further choices e.g. we could decide to include higher-order terms or to assume that $m(z)$ is modeled as an affine map and set $m_2 = 0$. The map m_{21} has to satisfy a further constraint if we assume that all trajectories approach the origin exponentially close to the slow manifold C^a_ϵ; this requires

$$k_2\sqrt{\epsilon} = (h^a_\epsilon \circ m_{21})(y,z).$$

Another constraint to generate MMOs is that the global map m_{21} maps some part of its domain close to the perturbation of the folded node funnel region. Although the model (11) has formally nine free parameters m_i, a_{jk}, b_l we can also view m_{21} as an $O(\epsilon)$-perturbation of the leading order term which has only two or three parameters depending on the choice of model ($m_2 = 0$ or $m_2 \neq 0$). Hence the description is low-dimensional, explicit and *decouples* the local and global bifurcation structure of the problem. To illustrate the effect of global bifurcation parameters we numerically investigate two typical MMO sequences, one for each local normal form with fixed local parameters.

Remark: In the following, we are going to visualize the LAOs in a time series for the dynamical system defined by m_{12} and m_{21} by inserting a large amplitude oscillation at fixed amplitude whenever the map m_{21} is applied.

For the folded node (15) we fix the parameters $(\epsilon, \mu) = (0.01, 0.006)$. Since $2k+1 < \frac{1}{\mu} < 2k+3$ for $k = 82$ we know from folded node theory that there will be $k + 2 = 84$ canards [10, 15]. The theory also predicts that the maximum number of small oscillations is $k + 1$. In Figure 9 we varied the global return mechanism to demonstrate that we can systematically reach sectors near a folded node with a sub-maximal number of oscillations and different MMO signatures. The global return map is chosen as the lowest order approximating linear map with $m(z) = 0.1z + m_0$ and $A = 0$, $b = 0$. The parameter m_0 is viewed as the main bifurcation parameter and controls the entry of trajectories to the different folded node rotation sectors. We find the following MMO signatures:

$m_0 =$	-0.015	-0.01	-0.005	-0.0025	-0.001	0.0
$L^s =$	1^{14}	1^9	1^4	1^2	2^1	1^0

Maximal MMO signatures can also be obtained but many of the small oscillations will be at an exponentially small scale due to the contraction towards the weak canard [15]. Observe that we

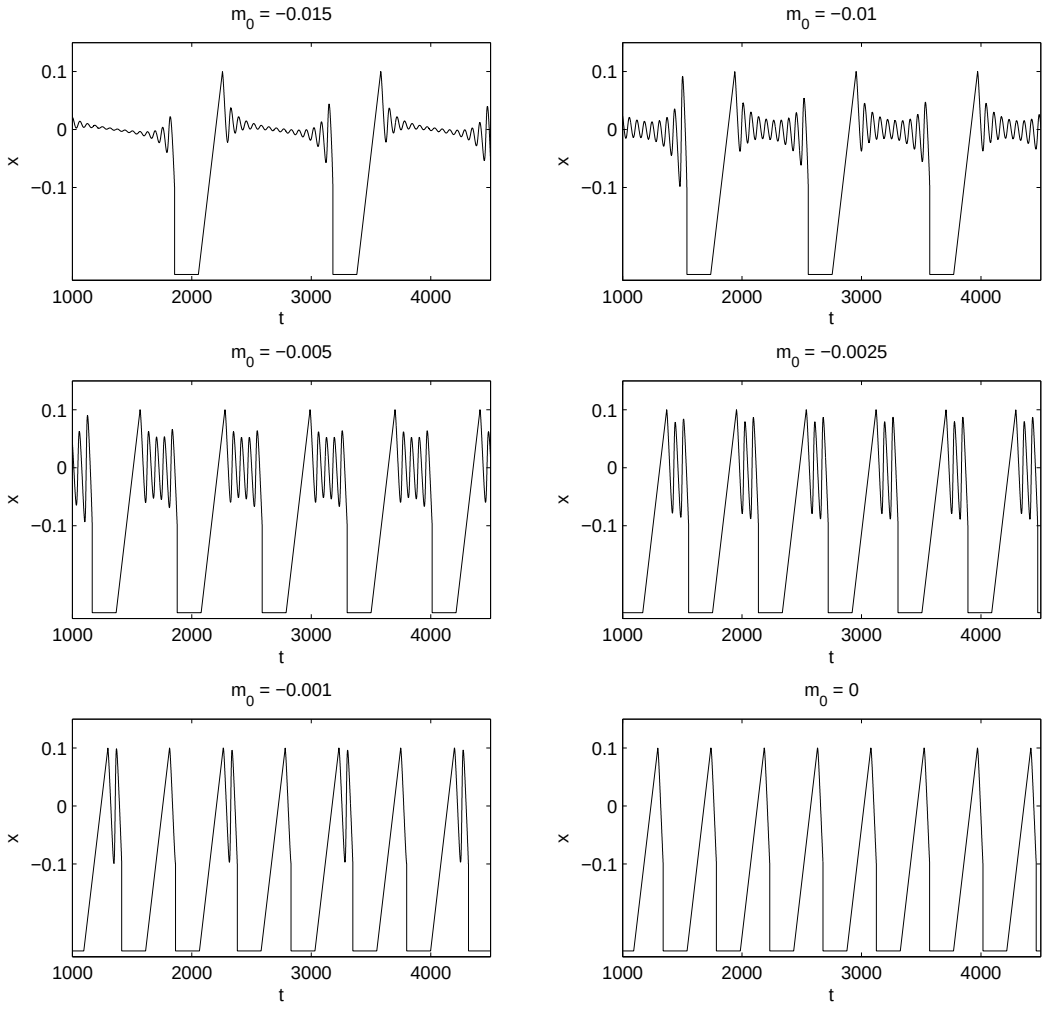

Figure 9: MMOs generated by the dynamical system with local dynamics (15) (parameters $\epsilon = 0.01$ and $\mu = 0.006$) and global dynamics $m(z) = 0.1z + m_0$ with $k_1 = \sqrt{\epsilon}$. The transition from local to global dynamics has been applied when $x < -\sqrt{\epsilon}$. Trajectories have been started at $(x, y, z) = (\sqrt{\epsilon}, \epsilon, 0.15)$.

have efficiently de-coupled the local parameter dynamics from the global parameter dynamics.

The second simulation focuses on the singular Hopf normal form (18). We fix the parameters $(\epsilon, \nu, a, b, c) = (0.01, 0.01, 0.5, -1, 1)$. For the global return map we again consider the singular limit of m_{21} with parameter $m_2 = 0$, $m_1 = 0.1$ and primary bifurcation parameter m_0. It is easy to check that the equilibrium near the fold curve is located at $q = (x_{eq}, y_{eq}, z_{eq}) \approx (-6.63729 \times 10^{-3}, 4.40537 \times 10^{-5}, -6.63729 \times 10^{-3})$. The equilibrium is a saddle-focus with one-dimensional stable and two-dimensional unstable manifold. We are in the regime where the SAOs are generated/amplified via the singular Hopf mechanism. Figure 10 shows the typical SAOs with increasing amplitude as they approach $W^u(q)$. We find the following MMO signatures:

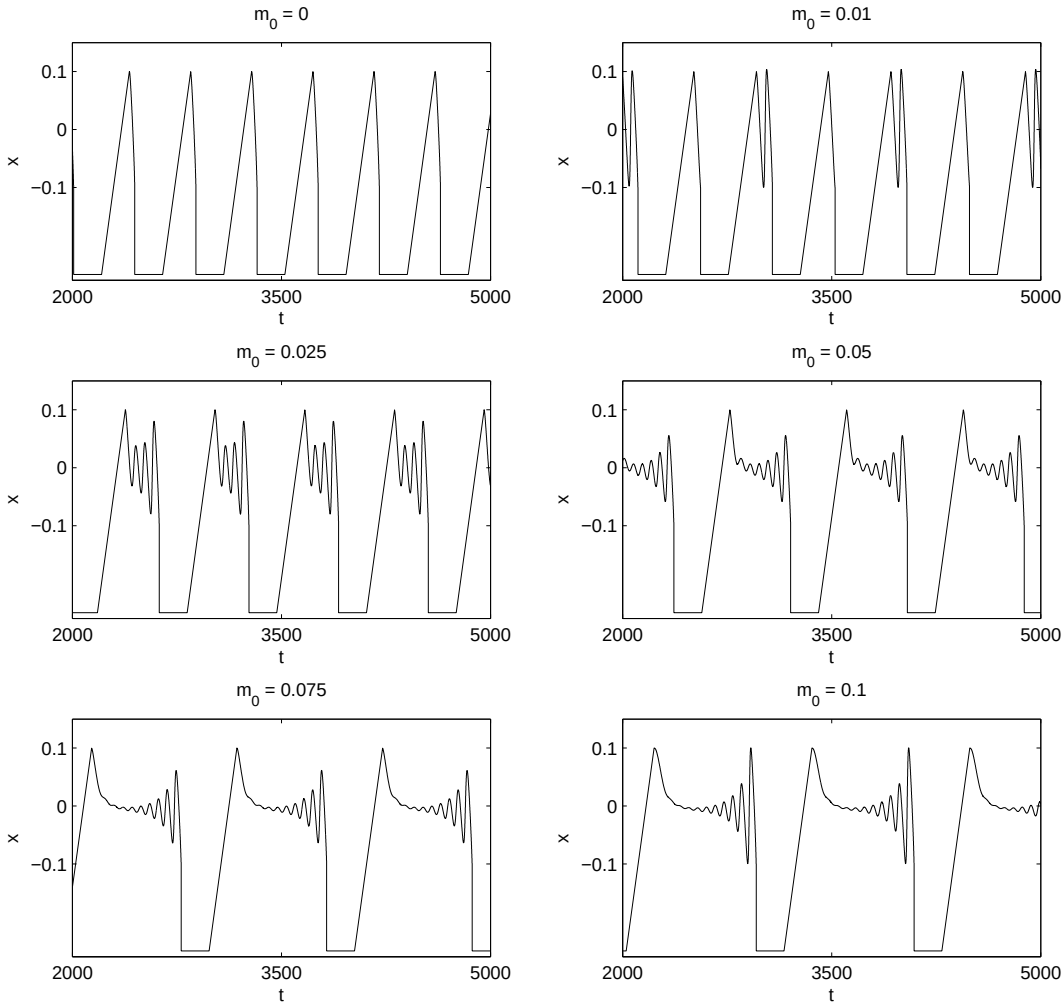

Figure 10: MMOs generated by the dynamical system with local dynamics (18) (parameters $(\epsilon, \nu, a, b, c) = (0.01, 0.015, 0.5, -1, 1)$) and global dynamics $m(z) = 0.1z + m_0$ with $k_1 = \sqrt{\epsilon}$. The transition from local to global dynamics has been applied when $x < -\sqrt{\epsilon}$. Trajectories have been started at $(x, y, z) = (\sqrt{\epsilon}, \epsilon, 0.15)$.

$m_0 =$	0.0	0.01	0.025	0.05	0.075	0.1
$L^s =$	1^0	2^1	1^3	1^6	1^9	1^9

It is important to note that the number of SAOs for the singular Hopf bifurcation is not only influenced by the folded node but also by the relative positions of the invariant manifolds of q [15]. In particular, Guckenheimer [29] points out that the one-dimensional stable manifold $W^s(q)$ seems to interact in an intricate way with MMO trajectories. Our decomposition approach is well-suited to investigate this dependency further once the local unfolding of the singular Hopf bifurcation is better understood [32]. Also for the singular Hopf bifurcation we have been able to reproduce a typical MMO sequence without varying the local parameters. Extensive additional numerical

simulation showed that it is difficult to produce periodic sequences of MMOs of the forms

$$L^s, \quad \text{with } L \gg 1, s \gg 1 \qquad \text{and} \qquad L_1^{s1} L_2^{s2} \cdots \tag{12}$$

by varying further parameters in the map $m(z)$. These simulations confirm parts of the incomplete theory for MMOs in three dimensions [47, 48] which predict the limited number of MMO patterns for three time scale systems. Therefore we conjecture that higher-dimensional return maps are more likely to account for more complicated MMOs of the form (12).

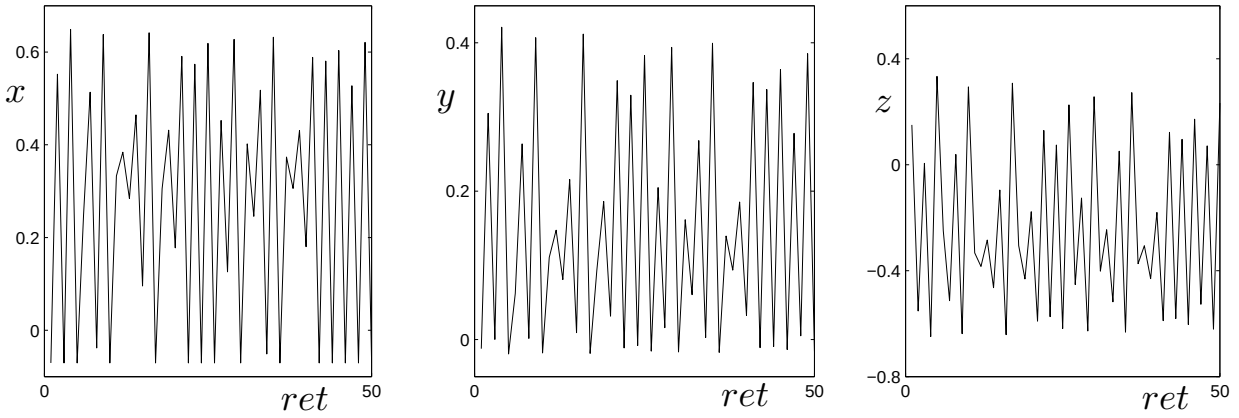

Figure 11: Coordinates (x, y, z) before the global map is applied; the horizontal axis shows the return number i.e. 1^{st} application of the global map, 2^{nd} application, etc. The entire orbits are generated by the dynamical system with local dynamics (18) (parameters $(\epsilon, \nu, a, b, c) = (0.01, 0.015, 0.5, -1, 1)$) and global dynamics $m(z) = 3z^2 + 0.2z - 0.8m_0$ with $k_1 = \sqrt{\epsilon}$. The transition from local to global dynamics has been applied when $x < -\sqrt{\epsilon}$. The times series of the returns shows typical chaotic non-periodic behavior.

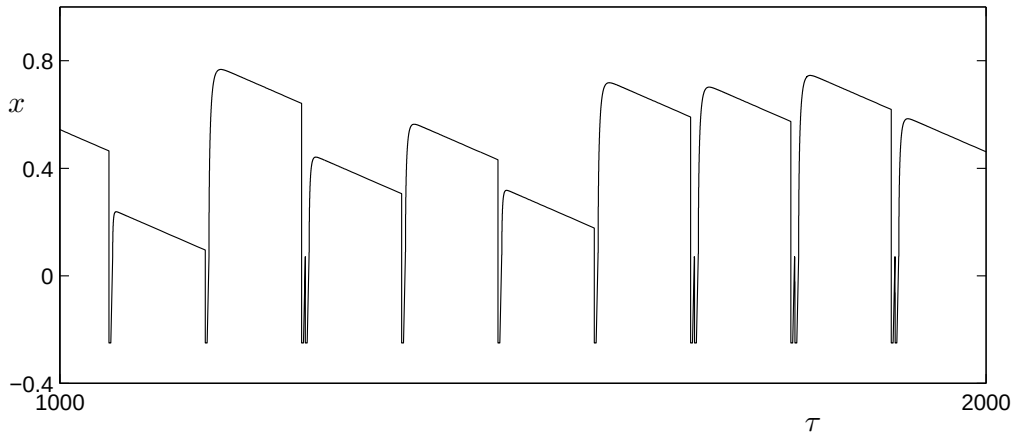

Figure 12: Subset of the time series in (x, τ) variables associated to the returns in Figure 11. Irregular oscillations are observed with 1^0 and 1^1 components.

Chaotic MMO signatures can be produced easily using a suitable quadratic map with $m_2 \neq 0$. Figures 11 and 12 illustrate an orbit obtained from the dynamical system of the singular Hopf bifurcation with global returns generated by the map $m(z) = 3z^2 + 0.2z - 0.8$; the irregular behavior of the global returns in Figure 11 suggests that this orbit is chaotic. It is well-known that

systems with two slow variables and one fast variable with S-shaped critical manifold can be chaotic [44, 36, 34, 57]. Koper [45] observed chaotic regions in parameter space in his original analysis of (2); transitions of MMOs to chaotic sequences can also be observed in many other models [15]. As shown above, our model is also able to reproduces this aspect of typical MMO models. We conclude that our modeling approach reproduces the main dynamical features and decouples the global parameter dynamics from the local parameter dynamics.

7 Brief Outlook

The strategy and methods we presented in this paper apply, in principle, to any system where the MMO mechanism can be decomposed into a local part that generates the SAOs and a global return map. For folded nodes and singular Hopf generated SAOs, the overall dimension can be arbitrary. Indeed, it has recently been shown by Wechselberger [72] that the local theory in Appendices A.2-A.3 extends to systems with $m \geq 1$ fast and $n \geq 2$ slow variables. The technique is to use a center manifold reduction to get into the situation $(m, n) = (1, 2)$. Then we can still compute singular return maps as we still have the three important one-dimensional curves that are analogous to L^{μ}, γ_s and F^{+} in the Koper model. We have resolved the map for the Koper model in more detail using the drop curves $L^{a\pm}$. However, we could just compute $m_{a,+} \circ m_j$ and $m_{a,+} \circ m_f$ as single maps for another system or adapt the finer global decomposition to the fast-slow geometry of the problem. Moreover, it is very important to point out that a center manifold reduction has been already used in a four-dimensional system with MMOs generated by folded nodes and singular Hopf bifurcations [11]. Our methods apply verbatim to the resulting three-dimensional system obtained in [11].

It is expected that the return maps for other systems can be more complicated. For example, just consider the situation for the Koper model but insert several non-trivial slow subsystem hyperbolic attractors on C^{a-}. Then the maps m_j and m_f may even have gaps since orbits can get trapped on persisting attractors on C^{a-}_{ϵ}. Computing singular maps for several well-known MMO models [15] and analyzing their structure is an interesting project but is beyond the scope of this paper.

Acknowledgment: I would like to thank two anonymous referees for valuable comments that helped to improve the focus and exposition of the paper.

A Background Review

A.1 Fast-Slow Systems

We are only going to recall the basic definitions and results about fast-slow systems. There are several standard references that detail many parts of the theory [40, 41, 60, 44, 27, 15, 1, 51]. A fast-slow system of ordinary differential equations (ODEs) is given by:

$$\begin{array}{rcccl} \epsilon\dot{x} & = & \epsilon\frac{dx}{d\tau} & = & f(x,y), \\ \dot{y} & = & \frac{dy}{d\tau} & = & g(x,y), \end{array} \tag{13}$$

where $x \in \mathbb{R}^m$ are fast variables, $y \in \mathbb{R}^n$ are slow variables and $0 < \epsilon \ll 1$ is a small parameter representing the ratio of time scales. Equation (13) can be re-written by changing from the slow

time scale τ to the fast time scale $t = \tau/\epsilon$

$$\begin{aligned} x' &= \tfrac{dx}{dt} = f(x,y), \\ y' &= \tfrac{dy}{dt} = \epsilon g(x,y). \end{aligned} \tag{14}$$

The singular limit $\epsilon \to 0$ of (14) yields the fast subsystem ODEs parametrized by the slow variables y. Setting $\epsilon \to 0$ in (13) gives a differential-algebraic equation (DAE), called the slow subsystem, on the critical manifold $C := \{f(x,y) = 0\}$. Concatenations of fast and slow subsystem trajectories are called candidates.

A subset $S \subset C$ is called normally hyperbolic if the $m \times m$ total derivative matrix $(D_x f)(p)$ is hyperbolic. A normally hyperbolic subset S is attracting if all eigenvalues of $(D_x f)(p)$ have negative real parts for $p \in S$; similarly S is called repelling if all eigenvalues have positive real parts. On normally hyperbolic parts of C the implicit function theorem applies to $f(x,y) = 0$ providing a map $h(y) = x$ so that C can be expressed (locally) as a graph. Fenichel's Theorem [24, 40, 69, 74] states that a compact normally hyperbolic submanifold $S = S_0$ of the critical manifold C perturbs for $\epsilon > 0$ sufficiently small, including stability and flow properties, to a slow manifold S_ϵ.

A trajectory is called a maximal canard if it lies in the intersection of an attracting and a repelling slow manifold. Canards were first investigated by a group of French mathematicians [5, 20, 4, 6] using nonstandard analysis. Later also asymptotic [23, 2, 44] and geometric [22, 49, 67] methods have been developed to understand canard orbits.

A.2 Folded Nodes

Normal hyperbolicity can fail in several ways. Here we briefly review the basic properties of two such situations [15]. A non-degenerate fold point $p \in C$ is defined by requiring that $f(p) = 0$ and $(D_x f)(p)$ has rank $m-1$ with left and right null vectors w and v so that $w \cdot [(D_{xx} f)(p)(v,v)] \neq 0$ and $w \cdot [(D_y f)(p)] \neq 0$. The set of fold points forms a manifold of codimension one in the m-dimensional critical manifold C. If $m = 1$ and $n = 2$ the fold points generically form a smooth curve that separates attracting and repelling sheets of the two-dimensional critical manifold C.

Two standard generating mechanisms for small oscillations near fold curves of the critical manifold will be considered in a normal form setup. Brøns, Krupa and Wechselberger [67, 10] consider a normal form

$$\begin{aligned} \epsilon \dot{x} &= y - x^2, \\ \dot{y} &= -(\mu+1)x - z, \\ \dot{z} &= \tfrac{\mu}{2}, \end{aligned} \tag{15}$$

where x is the fast variable, (y,z) are the slow variables and μ is a parameter. The critical manifold for (15) is $C = \{y = x^2\}$ with a line of fold points $F = \{x = 0, y = 0\}$. F decomposes the critical manifold $C = C^r \cup F \cup C^a$ where $C^r = C \cap \{x < 0\}$ is repelling and $C^a = C \cap \{x > 0\}$ is attracting. Differentiating $y = x^2$ implicitly with respect to τ gives $\dot{y} = 2x\dot{x}$. Therefore the slow flow is

$$\begin{aligned} \dot{x} &= \tfrac{-(\mu+1)x - z}{2x}, \\ \dot{z} &= \tfrac{\mu}{2}. \end{aligned} \tag{16}$$

Rescaling time by $\tau \mapsto 2x\tau$ reverses the direction of the flow on C^r and yields the desingularized slow flow

$$\begin{pmatrix} \dot{x} \\ \dot{z} \end{pmatrix} = \underbrace{\begin{pmatrix} -(\mu+1) & -1 \\ \mu & 0 \end{pmatrix}}_{=:A_0} \begin{pmatrix} x \\ z \end{pmatrix} \tag{17}$$

The desingularized slow flow has an equilibrium point at the origin $0 = (0, 0) \in F$ called a folded singularity. The eigenvalues $(\lambda_s, \lambda_w) = (-1, -\mu)$ of A_0 determine the type of the folded singularity. It is a folded saddle for $\mu < 0$, a folded node for $\mu > 0$ and a folded saddle-node of type II for $\mu = 0$ [67, 15]. We restrict to the folded node case and $\mu \in (0, 1)$ here. Then λ_s is associated to the strong eigendirection $\gamma_{s,0}$ and λ_w is associated to the weak eigendirection $\gamma_{w,0}$. The extension of $\gamma_{s,0}$ ($\gamma_{w,0}$) under the slow flow is referred to as the strong (weak) singular canard. Trajectories in the funnel region bounded by $\gamma_{s,0}$ and F can pass from C^a to C^r; see also [67, 10].

The singular canards $\gamma_{0,s}$ and $\gamma_{0,w}$ perturb to maximal canards $\gamma_{\epsilon,s}$ and $\gamma_{\epsilon,w}$ that lie in the intersection of the two slow manifolds $C^a_\epsilon \cap C^r_\epsilon$ [67]. If $1/\mu \notin \mathbb{N}$ then there are further maximal canards arising as intersections of $C^a_\epsilon \cap C^r_\epsilon$, called secondary canards [71]. In particular, the attracting and repelling invariant manifolds twist around each other [30, 28]. The number of twists of a trajectory in the fold region can be predicted using its distance δ relative to the strong singular canard and by the value of μ [10]. We agree to the convention that $\delta > 0$ indicates a trajectory entering the funnel region, $\delta = 0$ describes the strong canard and for $\delta < 0$ we are outside of the funnel. The twists can cause the SAOs of an MMO.

A.3 Singular Hopf

Note carefully that the normal form (15) has no global equilibrium point for $\mu \in (0, 1)$. However, in many applications a Hopf bifurcation occurs near the onset of MMOs [15] which suggests to consider the possibility of a global equilibrium point passing through the folded node region. In particular, one has to add higher-order terms to the equation for $\dot{z}$ in (15). Augmenting these terms it is well-known that the global equilibrium can undergo a Hopf bifurcation at an $O(\epsilon)$-distance from the fold curve. This scenario is also been referred to as singular Hopf bifurcation [8, 29] since the pair of complex conjugate eigenvalues involved in the Hopf bifurcation has a singular limit as $\epsilon \to 0$ [8]. Guckenheimer [29] derives the following normal form for a singular Hopf bifurcation

$$\begin{aligned} \epsilon\dot{x} &= y - x^2, \\ \dot{y} &= z - x, \\ \dot{z} &= -\nu - ax - by - cz, \end{aligned} \tag{18}$$

where x is a fast variable, (y, z) are slow variables and (ν, a, b, c) are parameters. The key difference between (15) and (18) is that we can find global equilibria $q = q(\nu, a, b, c)$ for (18). They are determined by solving the equation

$$-\nu = (a + c)x + bx^2. \tag{19}$$

If $\nu \approx 0$ then the equilibrium point is close to the folded singularity at the origin. The desingularized slow flow of (18) can be calculated similar to the folded node case. It can be shown [15, 50] that q is only important for the local dynamics near $(0, 0, 0)$ if ν is smaller than $O(\epsilon^{1/2})$. The key difference between MMOs that pass near a global equilibrium is that the SAOs can also be influenced by the stable and unstable manifolds $W^s(q)$ and $W^u(q)$. Detailed visualizations of the situation can be found in [15, 16]. Results for the unfolding of (18) can be found in [29, 32]. We are going to use the normal forms (15) and (18) as "black-box" units for numerical simulation in Section 6.

B Error Analysis

We briefly analyze the error of our approximation for the maps m_K for $K \in \{j, (a, +), b, f\}$ for $k = -10$ and $\lambda \in (\lambda_{FSN}, \lambda_{nf})$. The numerical integration of trajectories was carried out with a

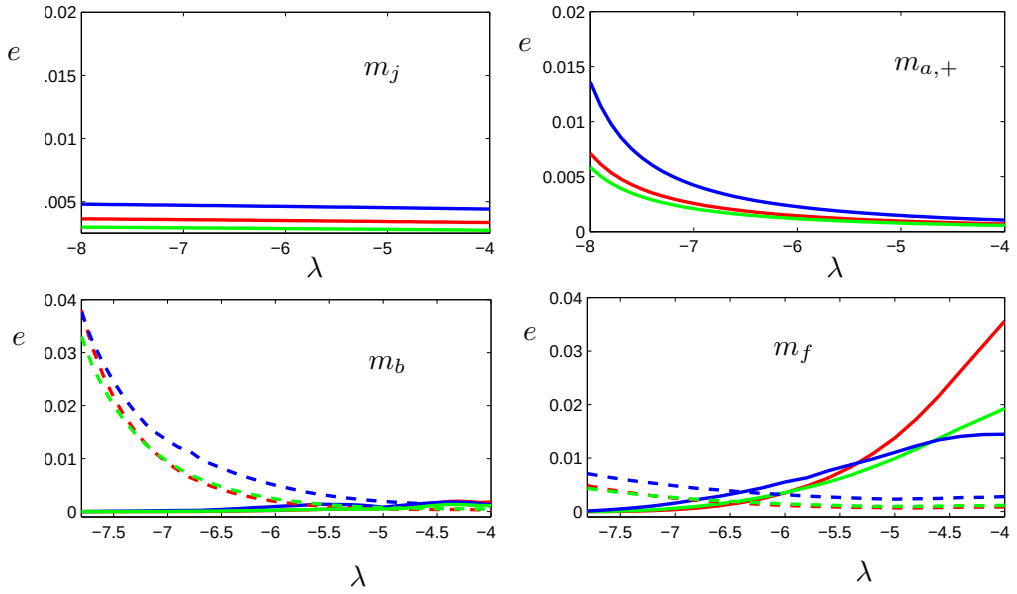

Figure 13: .Affine and quadratic fit approximation error e of the different maps m_K for $K \in \{j,(a,+),b,f\}$ given in (20). The horizontal axes are slices in λ-parameter space with $k=-10$. The error is measured in three different norms L^1 (red), L^2 (green) and L^∞ (blue). The dashed curves for m_b and m_f indicate the error for the lower branches and the solid curves the error for the upper branches of the maps. The domain for m_j and $m_{a,+}$ has been chosen as $z \in (2\lambda-(4+k)-1, 2\lambda-(4+k)+1)$ and the domain for m_b and m_f is the entire projection of the strong canard.

standard stiff numerical integration method (`ode15s` in MatLab [55]) with absolute error tolerance 10^{-8}. The grid size h for the domain of the maps m_K was always chosen so that $h \leq 0.02$. The main question we have to address is whether at a given fixed set of parameters (λ,k) there exist affine and quadratic approximations as postulated in Section 4. Figure 13 shows the error of the fit to the postulated polynomial forms measured in three different norms

$$\begin{aligned} e(L^1) &= \int_{z_0}^{z_1} |m_K^{num}(z) - m_K^{fit}(z)|dz, \\ e(L^2) &= \left(\int_{z_0}^{z_1} (m_K^{num}(z) - m_K^{fit}(z))^2 dz\right)^{1/2}, \\ e(L^\infty) &= \sup_{z\in[z_0,z_1]} |m_K^{num}(z) - m_K^{fit}(z)|, \end{aligned} \tag{20}$$

where m_K^{num} indicates the map obtained from numerical integration and m_K^{fit} denotes the affine and quadratic fits. The integrals in (20) have been evaluated from the discrete numerical integration data and the associated polynomials fits using a composite Simpson rule [65] which has error $\mathcal{O}(h^5)$ as $h \to 0$. Figure 13 shows that the worst-case error for the proposed affine and quadratic maps due is at most on the order of 10^{-2} over the entire range of parameters; the numerical integration error 10^{-8} and the numerical quadrature error $h^5 \leq (0.02)^5$ can be neglected here. Overall, the affine and quadratic approximations are certainly satisfactory to extract the basic MMO patterns.

A natural question is to ask what happens to the perturbations of m_K when $\epsilon > 0$. It is well-known from Fenichel theory that the error near normally hyperbolic segments of the critical manifold and in the fast subsystem is at most $\mathcal{O}(\epsilon)$ as $\epsilon \to 0$. Near the fold points [68] it has been proven that the error is at most $\mathcal{O}(\epsilon^{1/3})$ as $\epsilon \to 0$. Therefore we have that $m_K(z) + \mathcal{O}(\epsilon^{1/3})$ represents a flow map for $0 < \epsilon \ll 1$.

The numerical computations we present here can likely be made mathematically rigorous [36]

using interval arithmetic and tools such as IntLab [63]. The main reason for this conjecture is that rigorous numerical integration and quadrature are two standard situations in interval arithmetic [63]. However, carrying out this rigorous proof is beyond the scope and goals of this paper.

References

[1] V.I. Arnold. *Encyclopedia of Mathematical Sciences: Dynamical Systems V*. Springer, 1994.

[2] S.M. Baer and T. Erneux. Singular Hopf bifurcation to relaxation oscillations I. *SIAM J. Appl. Math.*, 46(5):721–739, 1986.

[3] D. Barkley. Slow manifolds and mixed-mode oscillations in the Belousov-Zhabotinskii reaction. *J. Chem. Phys.*, 89(9):5547–5559, 1988.

[4] E. Benoît. Systems lents-rapides dans $\mathbb{R}^3$ et leurs canards. In *Third Snepfenried geometry conference*, volume 2, pages 159–191. Soc. Math. France, 1982.

[5] E. Benoît, J.L. Callot, F. Diener, and M. Diener. Chasse au canards. *Collect. Math.*, 31:37–119, 1981.

[6] E. Benoît and C. Lobry. Les canards de $\mathbb{R}^3$. *C.R. Acad. Sc. Paris*, 294:483–488, 1982.

[7] J. Boissonade and P. DeKepper. Transitions from bistability to limit cycle oscillations. Theoretical analysis and experimental evidence in an open chemical system. *J. Phys. Chem.*, 84:501–506, 1980.

[8] B. Braaksma. Singular Hopf bifurcation in systems with fast and slow variables. *Journal of Nonlinear Science*, 8(5):457–490, 1998.

[9] M. Brøns, T.J. Kaper, and H.G. Rotstein. Introduction to focus issue - mixed mode oscillations: experiment, computation, and analysis. *Chaos*, 18:015101, 2008.

[10] M. Brøns, M. Krupa, and M. Wechselberger. Mixed mode oscillations due to the generalized canard phenomenon. *Fields Institute Communications*, 49:39–63, 2006.

[11] R. Curtu. Singular Hopf bifurcation and mixed-mode oscillations in a two-cell inhibitory neural network. *Physica D*, 239:504–514, 2010.

[12] H. Degn, L.F. Olsen, and J.W. Perram. Bistability, oscillation, and chaos in an enzyme reaction. *Annals of the New York Academy of Sciences*, 316(1):623–637, 1979.

[13] B. Van der Pol. A theory of the amplitude of free and forced triode vibrations. *Radio Review*, 1:701–710, 1920.

[14] B. Van der Pol. On relaxation oscillations. *Philosophical Magazine*, 7:978–992, 1926.

[15] M. Desroches, J. Guckenheimer, C. Kuehn, B. Krauskopf, H. Osinga, and M. Wechselberger. Mixed-mode oscillations with multiple time scales. *SIAM Rev. - in press*, 2012. http://rose.bris.ac.uk/dspace/handle/1983/1594.

[16] M. Desroches, B. Krauskopf, and H.M. Osinga. Mixed-mode oscillations and slow manifolds in the self-coupled FitzHugh-Nagumo system. *Chaos*, 18:015107, 2008.

[17] M. Desroches, B. Krauskopf, and H.M. Osinga. The geometry of mixed-mode oscillations in the Olsen model for the perioxidase-oxidase reaction. *DCDS-S*, 2(4):807–827, 2009.

[18] M. Desroches, B. Krauskopf, and H.M. Osinga. Numerical continuation of canard orbits in slow-fast dynamical systems. *Nonlinearity*, 23(3):739–765, 2010.

[19] C.T. Dickson, J. Magistretti, M.H. Shalisnky, B. Hamam, and A. Alonso. Oscillatory activity in entorhinal neurons and circuits: Mechanisms and function. *Ann. N.Y. Acad. Sci.*, 911:127–150, 2006.

[20] M. Diener. The canard unchained or how fast/slow dynamical systems bifurcate. *The Mathematical Intelligencer*, 6:38–48, 1984.

[21] E.J. Doedel, A. Champneys, F. Dercole, T. Fairgrieve, Y. Kuznetsov, B. Oldeman, R. Paffenroth, B. Sandstede, X. Wang, and C. Zhang. Auto 2007p: Continuation and bifurcation software for ordinary differential equations (with homcont). *http://cmvl.cs.concordia.ca/auto*, 2007.

[22] F. Dumortier and R. Roussarie. Canard cycles and center manifolds. *Memoirs of the American Mathematical Society*, 121(577), 1996.

[23] W. Eckhaus. Relaxation oscillations including a standard chase on french ducks. *Lecture Notes in Mathematics*, 985:449–494, 1983.

[24] N. Fenichel. Geometric singular perturbation theory for ordinary differential equations. *Journal of Differential Equations*, 31:53–98, 1979.

[25] A. Goryachev, P. Strizhak, and R. Kapral. Slow manifold structure and the emergence of mixed-mode oscillations. *J. Chem. Phys.*, 107(18):2881–2889, 1997.

[26] W.F. Govaerts. *Numerical Methods for Bifurcations of Dynamical Equilibria*. SIAM, 1987.

[27] J. Grasman. *Asymptotic Methods for Relaxation Oscillations and Applications*. Springer, 1987.

[28] J. Guckenheimer. Return maps of folded nodes and folded saddle-nodes. *Chaos*, 18:015108, 2008.

[29] J. Guckenheimer. Singular Hopf bifurcation in systems with two slow variables. *SIAM J. Appl. Dyn. Syst.*, 7(4):1355–1377, 2008.

[30] J. Guckenheimer and R. Haiduc. Canards at folded nodes. *Mosc. Math. J.*, 5(1):91–103, 2005.

[31] J. Guckenheimer and P. Holmes. *Nonlinear Oscillations, Dynamical Systems, and Bifurcations of Vector Fields*. Springer, 1983.

[32] J. Guckenheimer and P. Meerkamp. Bifurcation analysis of singular Hopf bifurcation in $\mathbb{R}^3$. *preprint*, 2011.

[33] J. Guckenheimer and C. Scheper. A geometric model for mixed-mode oscillations in a chemical system. *SIAM J. Appl. Dyn. Sys.*, 10(1):92–128, 2011.

[34] J. Guckenheimer, M. Wechselberger, and L.-S. Young. Chaotic attractors of relaxation oscillations. *Nonlinearity*, 19:701–720, 2006.

[35] J. Guckenheimer and A.R. Willms. Asymptotic analysis of subcritical Hopf-homoclinic bifurcation. *Physica D*, 139:195–216, 2000.

[36] R. Haiduc. Horseshoes in the forced van der Pol system. *Nonlinearity*, 22:213–237, 2009.

[37] T. Hauck and F.W. Schneider. Mixed-mode and quasiperiodic oscillations in the peroxidase-oxidase reaction. *J. Phys. Chem.*, 97:391–397, 1993.

[38] M.J.B. Hauser and L.F. Olsen. Mixed-mode oscillations and homoclinic chaos in an enzyme reaction. *J. Chem. Soc. Faraday Trans.*, 92(16):2857–2863, 1996.

[39] J.L. Hudson, M. Hart, and D. Marinko. An experimental study of multiple peak periodic and nonperiodic oscillations in the Belousov-Zhabotinskii reaction. *J. Chem. Phys.*, 71(4):1601–1606, 1979.

[40] C.K.R.T. Jones. Geometric singular perturbation theory. In *Dynamical Systems (Montecatini Terme, 1994)*, volume 1609 of *Lecture Notes in Mathematics*, pages 44–118. Springer, 1995.

[41] T.J. Kaper and C.K.R.T. Jones. A primer on the exchange lemma for fast-slow systems. *in: Multiple-Time-Scale Dynamical Systems*, IMA Vol. 122:65–88, 2001.

[42] A.L. Kawczynski, V.O. Khavrus, and P.E. Strizhak. Complex mixed-mode periodic and chaotic oscillations in a simple three-variable model of nonlinear system. *Chaos*, 10(2):299–310, 2000.

[43] A.L. Kawczynski and P.E. Strizhak. Period adding and broken Farey tree sequences of bifurcations for mixed-mode oscillations and chaos in the simplest three-variable nonlinear system. *J. of Chem. Phys.*, 112(14):6122–6130, 2000.

[44] E.F. Mishchenko Yu.S. Kolesov, A.Yu. Kolesov, and N.Kh. Rozov. *Asymptotic Methods in Singularly Perturbed Systems*. Plenum Press, 1994.

[45] M.T.M. Koper. Bifurcations of mixed-mode oscillations in a three-variable autonomous Van der Pol-Duffing model with a cross-shaped phase diagram. *Physica D*, 80:72–94, 1995.

[46] B. Krauskopf, H.M. Osinga, and J. Galán-Vique, editors. *Numerical Continuation Methods for Dynamical Systems: Path following and boundary value problems*. Springer, 2007.

[47] M. Krupa, N. Popovic, and N. Kopell. Mixed-mode oscillations in three time-scale systems: A prototypical example. *SIAM J. Applied Dynamical Systems*, 7(2), 2008.

[48] M. Krupa, N. Popovic, N. Kopell, and H.G. Rotstein. Mixed-mode oscillations in a three time-scale model for the dopaminergic neuron. *Chaos*, 18:015106, 2008.

[49] M. Krupa and P. Szmolyan. Extending geometric singular perturbation theory to nonhyperbolic points - fold and canard points in two dimensions. *SIAM J. Math. Anal.*, 33(2):286–314, 2001.

[50] M. Krupa and M. Wechselberger. Local analysis near a folded saddle-node singularity. *J. Diff. Eq.*, 248(12):2841–2888, 2010.

[51] C. Kuehn. *Multiple Time Scale Dynamics*. book in preparation, 2011.

[52] Yu.A. Kuznetsov. *Elements of Applied Bifurcation Theory - 3^{rd} edition*. Springer, 2004.

[53] J. Maselko and H.L. Swinney. A complex transition sequence in the Belousov-Zhabotinskii reaction. *Physica Scripta*, T9:35–39, 1985.

[54] J. Maselko and H.L. Swinney. Complex periodic oscillation and Farey arithmetic in the Belousov-Zhabotinskii reaction. *J. Chem. Phys.*, 85:6430–6441, 1986.

[55] The MathWorks. Matlab 2010b, 2010.

[56] G. Medvedev and Y. Yoo. Multimodal oscillations in systems with strong contraction. *Physica D*, 228:87–106, 2007.

[57] G. Medvedev and Y. Yoo. Chaos at the border of criticality. *Chaos*, 18:033105, 2008.

[58] A. Milik and P. Szmolyan. Multiple time scales and canards in a chemical oscillator. In C.K.R.T. Jones, editor, *Multiple Time Scale Dynamical Systems*, volume 122 of *The IMA Volumes in Mathematics and its Applications*, pages 117–140. Springer, 2001.

[59] A. Milik, P. Szmolyan, H. Loeffelmann, and E. Groeller. Geometry of mixed-mode oscillations in the 3-d autocatalator. *Int. J. of Bif. and Chaos*, 8(3):505–519, 1998.

[60] E.F. Mishchenko and N.Kh. Rozov. *Differential Equations with Small Parameters and Relaxation Oscillations (translated from Russian)*. Plenum Press, 1980.

[61] M. Orban and I.R. Epstein. Chemical oscillators in group VIA: The Cu(II)-catalyzed reaction between hydrogen peroxide and thiosulfate ion. *J. Am. Chem. Soc.*, 109:101–106, 1987.

[62] H.G. Rotstein, M. Wechselberger, and N. Kopell. Canard induced mixed-mode oscillations in a medial entorhinal cortex layer II stellate cell model. *SIAM J. Applied Dynamical Systems*, 7(4):1582–1611, 2008.

[63] S.M. Rump. Verification methods: rigorous results using floating-point arithmetic. *Acta Numerica*, 19:287–449, 2010.

[64] L.P. Shilnikov. A case of the existence of a denumerable set of periodic motions. *Sov. Math. Dokl.*, 6:163–166, 1965.

[65] J. Stoer and R. Bulirsch. *Introduction to Numerical Analysis*, volume 12 of *Texts in Applied Mathematics*. Springer, 2002.

[66] P.E. Strizhak and A.L. Kawczynski. Regularities in complex transient oscillations in the Belousov-Zhabotinsky reaction in a batch reactor. *J. Phys. Chem.*, 99:10830–10833, 1995.

[67] P. Szmolyan and M. Wechselberger. Canards in $\mathbb{R}^3$. *J. of Diff. Equat.*, 177:419–453, 2001.

[68] P. Szmolyan and M. Wechselberger. Relaxation oscillations in $\mathbb{R}^3$. *J. of Diff. Equat.*, 200:69–104, 2004.

[69] A.N. Tikhonov. Systems of differential equations containing small small parameters in the derivatives. *Mat. Sbornik N. S.*, 31:575–586, 1952.

[70] T.G.J. van Venrooij and M.T.M. Koper. Bursting and mixed-mode oscillations during the hydrogen peroxide reduction on a platinum electrode. *Electrochimica Acta*, 40(11):1689–1696, 1995.

[71] M. Wechselberger. Existence and bifurcation of canards in $\mathbb{R}^3$ in the case of a folded node. *SIAM J. Applied Dynamical Systems*, 4(1):101–139, 2005.

[72] M. Wechselberger. A propos de canards (apropos canards). *to appear in: Trans. Amer. Math. Soc.*, pages 1–20, 2011.

[73] M. Wechselberger and W. Weckesser. Bifurcations of mixed-mode oscillations in a stellate cell model. *Physica D*, 238:1598–1614, 2009.

[74] S. Wiggins. *Normally Hyperbolic Invariant Manifolds in Dynamical Systems*. Springer, 1994.